Environmental Science & Technology

Article

pubs.acs.org/est

Real-Time Studies of Iron Oxalate-Mediated Oxidation of Glycolaldehyde as a Model for Photochemical Aging of Aqueous Tropospheric Aerosols

Daniel A. Thomas,[†] Matthew M. Coggon,[‡,¶] Hanna Lignell,[‡,§] Katherine A. Schilling,[‡,∥] Xuan Zhang,[§] Rebecca H. Schwantes,[§] Richard C. Flagan,[‡,§] John H. Seinfeld,[‡,§] and J. L. Beauchamp*[,†]

[†]Arthur Amos Noyes Laboratory of Chemical Physics, California Institute of Technology, Pasadena, California 91125, United States
[‡]Division of Chemistry and Chemical Engineering, California Institute of Technology, Pasadena, California 91125, United States
[§]Environmental Science and Engineering, California Institute of Technology, Pasadena, California 91125, United States

Supporting Information

ABSTRACT: The complexation of iron(III) with oxalic acid in aqueous solution yields a strongly absorbing chromophore that undergoes efficient photodissociation to give iron(II) and the carbon dioxide anion radical. Importantly, iron(III) oxalate complexes absorb near-UV radiation (λ > 350 nm), providing a potentially powerful source of oxidants in aqueous tropospheric chemistry. Although this photochemical system has been studied extensively, the mechanistic details associated with its role in the oxidation of dissolved organic matter within aqueous aerosol remain largely unknown. This study utilizes glycolaldehyde as a model organic species to examine the oxidation pathways and evolution of organic aerosol initiated by the photodissociation of aqueous iron(III) oxalate complexes. Hanging droplets (radius 1 mm) containing iron(III), oxalic acid, glycolaldehyde, and ammonium sulfate (pH ~3) are exposed to irradiation at 365 nm and sampled at discrete time points utilizing field-induced droplet ionization mass spectrometry (FIDI-MS). Glycolaldehyde is found to undergo rapid oxidation to form glyoxal, glycolic acid, and glyoxylic acid, but the formation of high molecular weight oligomers is not observed. For comparison, particle-phase experiments conducted in a laboratory chamber explore the reactive uptake of gas-phase glycolaldehyde onto aqueous seed aerosol containing iron and oxalic acid. The presence of iron oxalate in seed aerosol is found to inhibit aerosol growth. These results suggest that photodissociation of iron(III) oxalate can lead to the formation of volatile oxidation products in tropospheric aqueous aerosols.

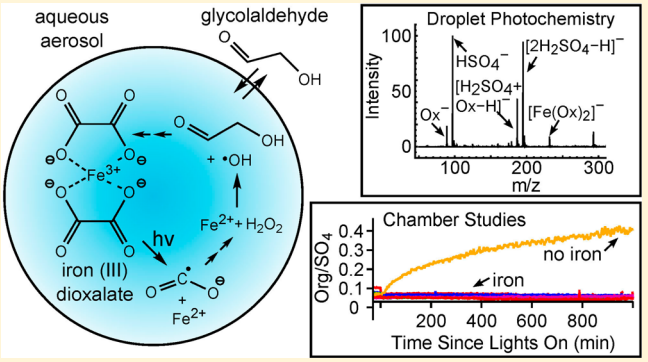

INTRODUCTION

Tropospheric aqueous-phase chemistry plays a key role in the aging of dissolved organics in the atmosphere.[1−5] Aqueous-phase processing may occur as a result of "dark" reactions such as acid catalysis, hydration, and oligomerization[6,7] or may result from photochemical excitation of dissolved light-absorbing species.[8−10] One of the key components directing the aging of dissolved organics is the availability of oxidative species such as the hydroxyl radical (OH) and hydrogen peroxide (H_2O_2), which may be present by direct generation in solution or by uptake from the gas phase.[11] Many laboratory studies have investigated secondary organic aerosol (SOA) production initiated by photolysis of dissolved H_2O_2.[12−15] There is increasing evidence, however, that processes involving the photolysis of photoactive organic and organometallic compounds may also be important sources of highly reactive aqueous oxidants.[9,16−18]

Transition metal ions present in cloudwater or aqueous aerosol are known to undergo photoinitiated electron transfer processes that can be a significant source of oxidative species.[1,19,20] Iron, the most abundant transition metal ion in tropospheric particles, can be found in aerosol particles originating from sea spray,[21] mineral dust,[20] and anthropogenic emissions.[22] Measured concentrations in fog waters range from micromolar or less in rural areas to tens of micromolar in highly polluted environments.[23] As a result of these significant concentrations, iron can play an important role in aqueous-phase tropospheric oxidation of organics. The reactions of dissolved iron-hydroxy complexes, or the Fenton reactions, are a well-characterized source of atmospheric oxidants.[24−26] The direct reaction of hydrogen peroxide with iron(III) yields hydroxyl radicals in the dark Fenton reaction 1, whereas the photo-Fenton reaction yields hydroxyl radicals by photolysis of the iron(III) hydroxy complex (reactions 2 and 3).

Received: July 20, 2016
Revised: October 3, 2016
Accepted: October 12, 2016
Published: October 12, 2016

DOI: 10.1021/acs.est.6b03588
Environ. Sci. Technol. 2016, 50, 12241−12249

$$Fe^{2+} + H_2O_2 \rightarrow Fe^{3+} + OH^{\bullet} + OH^{-} \quad (1)$$

$$Fe^{3+} + 2H_2O \leftrightarrow Fe(OH)^{2+} + H_3O^{+} \quad (2)$$

$$Fe(OH)^{2+} \xrightarrow{h\nu} Fe^{3+} + OH^{\bullet} \quad (3)$$

Several groups have recently explored the impact of iron photochemistry on SOA formation. Chu and co-workers studied the effects of iron(II) sulfate and iron(III) sulfate seed aerosol on SOA formation at 50% relative humidity (RH) and found that iron(II) complexes inhibited SOA formation, whereas iron(III) had little effect on SOA formation.[27] They attributed the effect of iron(II) to the reduction of organic condensate by the iron species and subsequent disruption of oligomerization processes. Nguyen and co-workers investigated the uptake and oxidation of glycolaldehyde in aqueous aerosol containing hydrogen peroxide and iron complexes.[26] They found that the photo-Fenton reaction significantly increased the degree of oxidation in aerosol particles when compared with H_2O_2 photolysis alone (ratio of O/C = 0.9 with iron and H_2O_2 vs O/C = 0.5 with H_2O_2).

Although laboratory experiments have demonstrated that photo-Fenton chemistry can lead to significant oxidation of organics,[28−30] the role of such processes in atmospheric aerosol is not clear, as the reactions are highly dependent on pH, iron concentration, and the concentration of other ligands that readily complex with iron.[25,31,32] Notably, the formation of stable complexes between iron and dicarboxylate ligands can have a significant impact on the photochemical reaction pathways. Complexation between the oxalate anion, one of the most abundant low-molecular weight organic compounds found in aqueous aerosol,[22,33−35] and iron has long been known to generate significant yields of oxidative species by photochemical reduction of iron. Initially studied as a chemical actinometer,[36,37] seminal work by Zuo and Hoigné demonstrated that photolysis of iron-oxalate complexes could lead to the generation of oxidative species under atmospherically relevant conditions.[25]

The proposed pathway for the photochemical generation of oxidative species from iron(III) oxalate complexes is shown in reactions 4-10 below. Depending on the pH, ionic strength, and concentration of iron and oxalate, three complexes are formed: $Fe(C_2O_4)^{+}$, which has low photochemical reactivity,[38] and $Fe(C_2O_4)_2^{-}$ and $Fe(C_2O_4)_3^{3-}$, both of which undergo photochemical reduction of iron with high quantum yield.[31,39] The mechanism of photochemical dissociation of $Fe(C_2O_4)_3^{3-}$ has been investigated in detail, with two groups presenting evidence for either intermolecular electron transfer (4a) or intramolecular electron transfer (4b) as the primary reaction pathway.[40−43] The mechanism of dissociation of $Fe(C_2O_4)_2^{-}$ has not been studied extensively but is also expected to yield the oxalate anion radical, which rapidly dissociates to CO_2 and $CO_2^{\bullet-}$ (reactions 5 and 6).[25] The subsequent reaction of $CO_2^{\bullet-}$ with O_2 leads to the eventual formation of H_2O_2 (reactions 7−9), which can then interact directly with Fe^{2+} (reaction 1) or with FeC_2O_4 (reaction 10) to produce OH.[44]

$$Fe(C_2O_4)_3^{3-} \xrightarrow{h\nu} Fe(C_2O_4)_2^{2-} + C_2O_4^{\bullet-} \quad (4a)$$

$$Fe(C_2O_4)_3^{2-} \xrightarrow{h\nu} Fe(C_2O_4)_2^{-} + 2CO_2^{\bullet-} \quad (4b)$$

$$Fe(C_2O_4)_2^{-} \xrightarrow{h\nu} Fe^{2+} + C_2O_4^{2-} + C_2O_4^{\bullet-} \quad (5)$$

$$C_2O_4^{\bullet-} \rightarrow CO_2^{\bullet-} + CO_2 \quad (6)$$

$$CO_2^{\bullet-} + O_2 \rightarrow CO_2 + O_2^{\bullet-} \quad (7)$$

$$O_2^{\bullet-} + H_3O^{+} \rightarrow HO_2^{\bullet} + H_2O \quad (8)$$

$$2HO_2^{\bullet} \rightarrow H_2O_2 + O_2 \quad (9)$$

$$FeC_2O_4 + H_2O_2 \rightarrow FeC_2O_4^{+} + OH^{\bullet} + OH^{-} \quad (10)$$

Although the mechanism and kinetics of dissociation of iron(III) oxalate complexes have been examined in detail, much less information is available on the oxidation of atmospherically relevant compounds by this photochemical system. Zuo and Zhan found that the presence of iron(III) oxalate complexes increases the rate of oxidation of sulfur dioxide compared to iron alone under atmospherically relevant conditions.[45] In field sampling studies, Sorooshian et al. found an inverse correlation between concentrations of dissolved iron and oxalate in stratocumulus cloudwater above the northeastern pacific ocean, suggesting that ferrioxalate photochemistry may play an important role in determining cloudwater composition under certain conditions.[22] These studies serve as initial demonstrations of the potential importance of such reactions in aqueous tropospheric chemistry, but further laboratory and field studies are necessary to better discern the complex interplay of reactions influencing the oxidation of dissolved organic compounds.

Glycolaldehyde serves as an excellent model system to study the influence of liquid-phase ferrioxalate photochemistry on the oxidation of dissolved organics. A major product of isoprene oxidation, glycolaldehyde is produced with an estimated global flux greater than 42 Tg C $year^{-1}$.[13,46,47] The abundance of glycolaldehyde, along with its high solubility,[48] means that its oxidation processes may play a significant role in the formation of SOA in aqueous aerosol.

This study explores the photochemically initiated reaction pathways involved in the oxidation of aqueous glycolaldehyde in the presence of ferrioxalate complexes. Real-time studies of photochemical reactions in microliter droplets utilizing field-induced droplet ionization mass spectrometry (FIDI-MS)[49,50] provide insight into the changes in chemical composition of this model system upon UV irradiation. Complementary particle-phase environmental chamber experiments[51,52] examine the evolution of iron-doped aqueous aerosol in the presence of gas-phase glycolaldehyde under simulated atmospheric conditions.

EXPERIMENTAL SECTION

Field-Induced Droplet Ionization Mass Spectrometry.

The FIDI-MS source employed in this study is based upon an initial design described by Grimm and co-workers.[50] The general design and features of the updated source are described here, with further details given in the Supporting Information. A hanging droplet of 1.5−2 mm in diameter (2−4 μL) is suspended on the end of a stainless steel capillary between two parallel plate electrodes separated by 6.3 mm (Figure 1c). The parallel plates are mounted to a translation stage to allow alignment of an aperture in the electrically grounded plate with the atmospheric pressure inlet of an LTQ-XL mass spectrometer (Thermo-Fisher, Waltham, MA). The capillary is mounted on a separate translation stage to provide for placement of the droplet midway between the two plates in alignment with the inlet of the LTQ-XL. A droplet is formed from liquid fed through the capillary using a motorized syringe

DOI: 10.1021/acs.est.6b03588
Environ. Sci. Technol. 2016, 50, 12241−12249

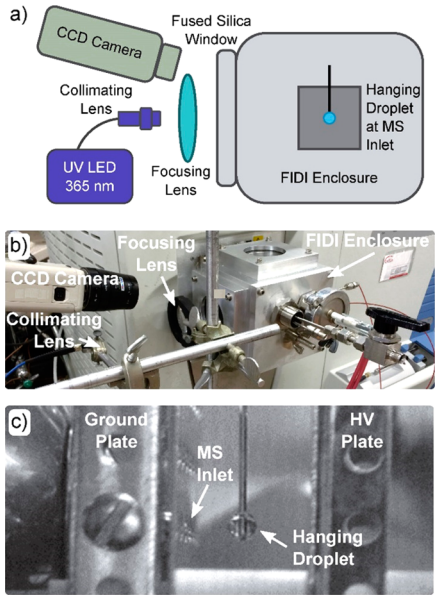

Figure 1. Experimental apparatus for studying photochemistry utilizing FIDI-MS. The primary components of the system are depicted schematically in panel a and shown as utilized in the laboratory in panel b. A CCD camera image of the FIDI region is shown in panel c.

pump. Mass spectrometric sampling of the hanging droplet is accomplished by application of a pulsed high voltage (3−5 kV, 100 ms duration) to the back parallel plate and to the suspended capillary at half the magnitude applied to the back plate to maintain field homogeneity between the electrodes. When a sufficiently high voltage is applied, the electrical forces overcome the surface tension of the droplet, resulting in the bipolar ejection of highly charged progeny droplets of less than 1 μm in diameter from opposite ends of the suspended droplet.[49,53] Charged droplets of a specific polarity enter the transfer capillary of the mass spectrometer, resulting in the detection of gas-phase ions in a manner similar to electrospray ionization (ESI).[54,55] Sampling of either positive or negative ions is achieved by switching the polarity of the high voltage applied to the back plate and capillary. The pulsed high voltage is controlled by a custom power supply and software described elsewhere.[56]

The entire FIDI source is mounted within a custom enclosure that allows for control of the environment in which the droplet is suspended, as shown in Figure 1a,b. The enclosure is equipped with a fused silica window to allow for the study of photochemical reactions and for visual droplet monitoring during experiments. To study the photochemistry of suspended droplets in the absence of oxygen, the chamber was flushed with nitrogen at a flow rate of 1.2 L/min for ∼10 min prior to sampling, and the flow of nitrogen was maintained throughout the experiment; the sample was also degassed by bubbling with nitrogen. For all other experiments undertaken in this work, the enclosure was left open to laboratory air. Photochemical reactions in the hanging droplet are accomplished by irradiation with 365 nm light generated by a fiber optic-coupled LED (FCS-0365−000, Mightex Systems, Pleasanton, CA). The light is focused onto the droplet using a collimating lens (74-UV, Ocean Optics, Dunedin, FL) coupled to a spherical focusing lens. A radiant flux of 760 ± 5 μW was measured at the location of the hanging droplet with use of a thermal power sensor (S302C, ThorLabs, Newton, NJ) coupled to a power and energy meter (PM100USB, ThorLabs). This measurement yields an upper limit of 1.4×10^{15} photons cm^{-2} s^{-1} on the photon flux encountering the hanging droplet, approximately 1 order of magnitude greater than the solar actinic flux at 365 nm with a 30° solar zenith angle.[57]

Photochemical experiments employing FIDI-MS were performed in solutions containing 0.5 mM H_2SO_4, 100 μM NH_3, 50 μM $FeCl_3$, 250 μM oxalic acid, and 250 μM glycolaldehyde. Control experiments were also performed by excluding iron, oxalic acid, or glycolaldehyde from the mixture. In a typical experiment, a droplet of the solution was formed on the end of the capillary and allowed to rest for 1 min prior to exposure to 365 nm radiation. Individual droplets were then sampled by application of a high voltage pulse after 0−3 min of irradiation. The presented spectra are averaged from four experiments on discrete droplets at each time point. Between experiments, the sample line was rinsed thoroughly with 10 mM H_2SO_4 to prevent the accumulation of iron precipitates.

Aerosol Chamber Instrumentation. Aerosol size distributions were measured with a custom-built scanning mobility particle sizer (SMPS) consisting of a differential mobility analyzer (model 3081, TSI, Shoreview, MN) coupled to a condensation particle counter (model 3010, TSI). Bulk aerosol composition was monitored by a high-resolution time-of-flight Aerodyne Aerosol Mass Spectrometer (HR-AMS). The principles and details of the HR-AMS are described elsewhere.[58,59] Prior to experiments, the instrument's ionization efficiency was calibrated with 350 nm NH_4NO_3 particles. The instrument was operated in V-mode, and data were analyzed following the recommendations of Aiken et al. and Canagaratna et al.[60,61]

Volatile organic compounds (VOCs) were monitored by a custom-built chemical ionization mass spectrometer (CIMS) with CF_3O^- reagent ions.[62,63] The instrument was primarily operated in negative mode, which allows for the detection of analyte $[R]$ and reagent clusters $[R{\cdot}CF_3O]^-$. For strongly acidic species $[H{\cdot}X]$, the transfer product $[H{\cdot}X{\cdot}F]^-$ is detected. For select species such as glycolaldehyde, the instrument was operated in tandem mass spectrometry (MS/MS) mode.[63] In this arrangement, a parent ion selected by the first quandrupole is exposed to elevated pressure of N_2 and fragmented into daughter ions that correspond to a unique compound at a common unit mass. Here, the daughter ion of the m/z 145/85 cluster is taken to reflect the glycolaldehyde signal.

Gas-phase concentrations of O_3 and NO + NO_2 (NO_x) were measured by Horiba (model APOA-360) and Teledyne monitors (model T200), respectively. The temperature and RH were monitored by Vaisala probes.

Aerosol Chamber Experimental Protocol. Experiments were performed in the Caltech dual 24 m^3 Teflon chambers.[51,52] Prior to each experiment, the chamber was flushed with air scrubbed by activated carbon, silica gel, Purafil media, and molecular sieves to achieve a particle background <10 cm^{-3}, O_3 background <10 ppb, and NO_x background <5 ppb. Once cleaned, chamber air was humidified to ≥80% relative humidity (RH) using a water circulator coupled to a Nafion membrane humidifier. Aerosols were injected into the chamber through a wet-walled humidifier; consequently, particles are assumed to be deliquesced. All experiments were conducted at 25 °C. Further details of the aerosol chamber experimental protocol can be found in the Supporting Information.

DOI: 10.1021/acs.est.6b03588
Environ. Sci. Technol. 2016, 50, 12241−12249

All experiments were performed in the presence of aerosol and gas-phase glycolaldehyde at low-NO_x and low-HO_x conditions (Table 1). Typical gas-phase oxidants (e.g., O_3, OH, NO) were not purposely injected into the chamber, and the resulting chemistry is therefore attributed to glycolaldehyde photolysis and interactions between volatilized glycolaldehyde and particles. Over the course of an experiment, NO_x levels never rose above the detection limits of the Teledyne monitors. Ozone rose slightly (~10 ppb) after photochemistry was induced, suggesting that low, pre-existing NO_x concentrations were present in the chamber.

Table 1. Experimental Conditions Summarizing Atomizer Solution Composition ($[Fe]_0$, $[Oxalate]_0$, pH), Initial Glycolaldehyde Concentrations, and Chamber Relative Humidity[a]

exp. number and description[b]		$[Fe]_0$ (μM)	$[oxalate]_0$ (μM)	pH	$[Gly]_0$ (ppb)	RH (%)
1	no seed	0	0		85	88
2	AS + Gly	0	500	3	83	85
3	0.005% Fe + Gly	2	500	3	97	90
4	0.03% Fe + Gly	10	500	3	93	87
5	0.3% Fe + Gly	100	500	3	81	94
6	5% Fe + Gly	2000	500	3	100	92

[a]All atomizer solutions contain 0.015 M ammonium sulfate (AS) and sulfuric acid added to achieve a pH of 3. [b]Aerosol iron content is represented as the percentage of total inorganic aerosol mass.

The aerosol seed composition was varied to investigate the impact of iron interactions on the uptake and particle-phase oxidation of glycolaldehyde (Table 1). Varying concentrations of iron(II) sulfate and oxalic acid were added to atomizer solutions of 0.015 M ammonium sulfate. The pH of the solutions was adjusted with 10 wt % sulfuric acid to an initial pH of 3 as measured by an Orion pH meter (Thermo-Fisher, Waltham, MA). We expect the pH to quickly change since the photochemistry of ferrioxalate systems is known to consume and generate hydronium ions. Solutions were prepared fresh daily to avoid the slow formation of iron(III) oxide from the reaction of dissolved iron(II) with oxygen. Experiments in the absence of iron were performed first to avoid the possibility of iron contamination within the atomizer, on chamber walls, and along sampling lines.

Iron concentrations were chosen to reflect a range of iron content observed in atmospheric water. Iron mass fractions in aerosol ranging from 3.5 to 7.7% have been reported,[23] and iron solubilities in atmospheric waters are reported to range between 0.018 and 22%. For example, measurements on ambient cloudwater samples found soluble iron concentrations as high as 0.57 μM,[64] and concentrations up to 1.3 μM were observed in samples impacted by shipping emissions.[22] On the basis of this wide range of soluble iron content, we doped our atomizer solutions with 2, 10, 100, or 2000 μM of iron, which correspond to inorganic weight fractions of 0.005, 0.03, 0.3, and 5%, respectively. Assuming that the aerosol exhibits hygroscopic properties similar to pure ammonium sulfate, we expect atomizer solutions to concentrate by approximately 2 orders of magnitude;[65] thus, these conditions reflect systems analogous to wet aerosol as opposed to the dilute cloudwater systems described above. Given the high concentrations of oxalate observed in atmospheric waters (up to ~0.12 μg m^{-3}),[22] particles were also doped with oxalate concentrations comparable to that of iron (500 μM). We limit our interpretation of chamber data to trends associated with iron doping. Future studies may consider the effect of oxalate in comparison to other organic acids.

Photochemical Box Model. A photochemical box model is employed to investigate glycolaldehyde losses due to gas-phase processes. Equations describing glycolaldehyde photolysis and reaction with OH are outlined in the Supporting Information. The photochemical model was initiated with a glycolaldehyde concentration of 85 ppb (exp. 1, Table 1).

RESULTS AND DISCUSSION

Photochemistry of Iron(III) Oxalate Complexes and Glycolaldehyde by FIDI-MS. Figure 2 shows the FIDI-MS spectra of hanging droplets containing iron(III) oxalate complexes and glycolaldehyde exposed to irradiation at 365 nm for 0–3 min. The HSO_4^- anion and its dimer are the most prominent ions in the spectrum due to the high concentration of sulfate in solution (0.5 mM) utilized to achieve a pH of ~3. Oxalic acid (Ox) is also detected prior to irradiation (0 min) as a monomer, homodimer, and heterodimer with hydrogen sulfate (m/z 89, 179, and 187, respectively), and the heterodimer of glycolaldehyde hydrate (glycol+H_2O) with hydrogen sulfate is also observed at m/z 175. The $Fe(C_2O_4)_2^-$ ion, predicted by equilibrium calculations to be the dominant complex of iron(III) in the sample (Figure S4), is detected at m/z 232. Upon irradiation, the $Fe(C_2O_4)_2^-$ complex and oxalic acid ions are rapidly depleted, and new ions are observed at m/z 173, 175, and 191. These photochemical oxidation products

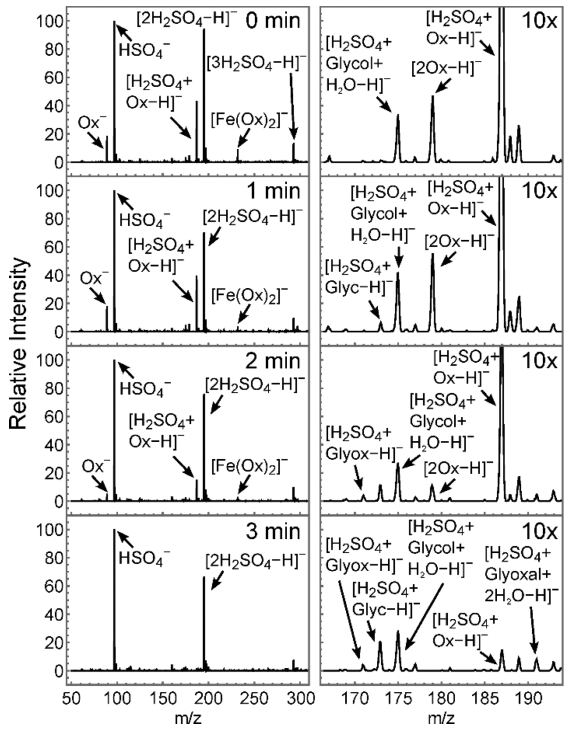

Figure 2. Monitoring the photochemistry of aqueous glycolaldehyde and iron(III) oxalate complexes by FIDI-MS. The left column shows the full spectrum, and the right column highlights the region where glycolaldehyde and its oxidation products are detected (10× zoom). The depletion of $Fe(C_2O_4)_2^-$ and oxalic acid (Ox) are clearly observed over the course of 3 min, and the oxidation of glycolaldehyde (glycol) to glycolic acid (glyc), glyoxylic acid (glyox), and glyoxal is observed.

DOI: 10.1021/acs.est.6b03588
Environ. Sci. Technol. 2016, 50, 12241–12249

are assigned to glycolic acid (glyc, m/z 173), glyoxylic acid (glyox, m/z 171), and glyoxal dihydrate (m/z 191), all observed as adducts with hydrogen sulfate. Formic acid is also observed as a dimer with hydrogen sulfate at m/z 143 with low intensity after 3 min of irradiation. It is possible that these ions represent the formation of organosulfate compounds rather than noncovalent complexes, but the free glycolic acid and glyoxylic acid ions (m/z 73 and 75, respectively), also increase in intensity over the course of the experiment, suggesting that the observed species are likely adducts formed during gas-phase ion generation.[14] The formation of these product ions is not observed in control experiments in which iron, glycolaldehyde, or oxalic acid is excluded from the reaction mixture (Figures S5 and S6).

The observed chemistry of the glycolaldehyde-ferrioxalate systems is summarized in Scheme 1. As described in reactions 4-10, photodissociation of iron oxalate complexes leads to the formation of hydroxyl radicals that oxidize glycolaldehyde to form glyoxal and glycolic acid. Further oxidation yields formic acid and glyoxylic acid from glycolaldehyde and glycolic acid, respectively. Glyoxylic acid may then undergo one final oxidation process to regenerate oxalic acid, whereas formic acid oxidation leads to the formation of carbon dioxide. Alternatively, hydrated glyoxal, detected prominently in FIDI-MS experiments in agreement with previous equilibrium measurements,[66−68] can be oxidized to glyoxylic acid hydrate and subsequently to oxalic acid.[4] The branching ratios of each pathway are challenging to determine within the current experiment, as the signal intensity in FIDI, similar to ESI, does not depend linearly on the molecule concentration in solution and thus provides only semiquantitative measurement.[54] The observed oxidation pathways are similar to those observed by Perri and co-workers for the oxidation of aqueous glycolaldehyde by hydroxyl radicals produced by H_2O_2 photolysis initiated by a 254 nm Hg lamp.[13] They also observed higher molecular weight oligomers in significant abundance and identified malonic and succinic acid as two of the major oligomerization products. Further study by Ortiz-Montalvo and co-workers identified malic and tartaric acids as additional oligomerization products.[69] Similarly, in a study of aerosol formation from reactive uptake of glycolaldehyde on seed aerosol doped with iron and H_2O_2, Nguyen and co-workers proposed that oligimerization products of glycolaldehyde contributed to the high observed O/C ratios of aerosol organics.[26] In contrast, the FIDI-MS experiments presented in this study did not detect the formation of any oligomers in significant abundance. The comparatively high flux of oxidative species produced by the photodissociation of iron(III) oxalate complexes may favor sequential oxidation over oligomerization under the conditions utilized in this study.

Scheme 1. Oxidation Pathway of Glycolaldehyde in the Presence of Iron(III) Oxalate Complexes

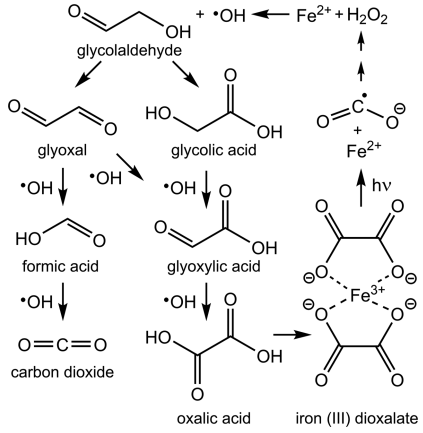

Photochemistry of Iron Oxalate and Glycolaldehyde in Deoxygenated Environment. The photochemistry of the iron(III) oxalate and glycolaldehyde system was also investigated in the absence of oxygen by purging both the sample solution and the reaction chamber with nitrogen gas. As shown in Figure 3, little change in the composition of the droplets is observed during irradiation under such conditions. In contrast to the nearly complete depletion of oxalate in the presence of oxygen, the ions associated with oxalic acid only marginally decrease in intensity over the course of the reaction. In addition, the intensity of the $Fe(C_2O_4)_2^-$ is significantly diminished after 1 min of irradiation, and little oxidation of glycolaldehyde is observed.

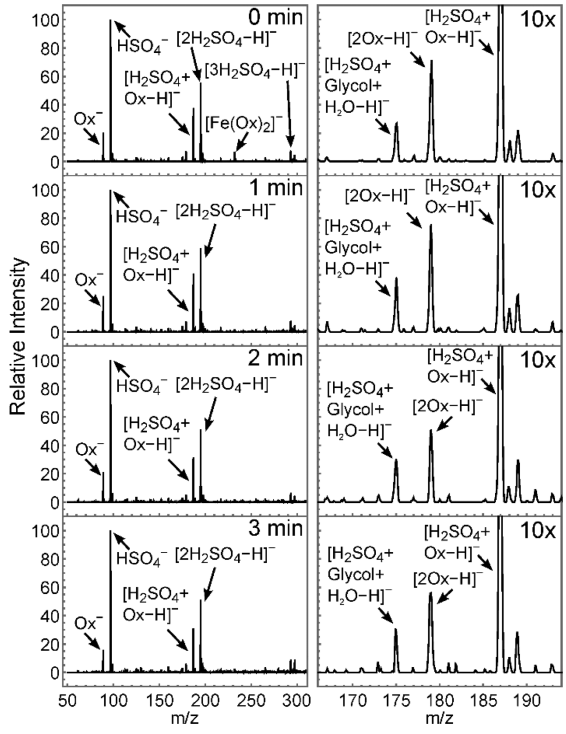

Figure 3. Photochemistry of deoxygenated solutions of iron(III) oxalate and glycolaldehyde. The full spectrum is shown on the left, and the right column shows a 10× zoom on the region of detection for glycolaldehyde and its oxidation products. In the absence of dissolved oxygen, little oxidation of glycoldaldehyde is observed, and oxalate is not depleted through the course of the experiment. The $Fe(C_2O_4)_2^-$ ion is significantly depleted after 1 min of irradiation.

The absence of glycolaldehyde oxidation products in deoxygenated solutions is readily explained by the necessity of oxygen for the generation of hydroxyl radicals as detailed in reactions 4−10. The small amount of oxidation observed is attributed to trace concentrations of oxygen gas in the enclosed reaction environment. The presence of oxygen is also necessary for the regeneration of iron(III) following photocatalyzed reduction. Weller and co-workers recently measured a quantum yield of 0.8 ± 0.1 for iron(II) formation under conditions similar to those utilized in this study, indicating that iron(III)

DOI: 10.1021/acs.est.6b03588
Environ. Sci. Technol. 2016, 50, 12241−12249

should be rapidly depleted in the absence of oxygen.[31] Consistent with this result, we do not observe the $Fe(C_2O_4)_2^-$ ion following irradiation in a nitrogen atmosphere. Similarly, little change in the intensity of oxalate ions is observed, as only 20−30% of the oxalic acid can be dissociated before all of the iron present is reduced. Zuo and Hoigne also observed that nearly all of the iron(III) was reduced to iron(II) rapidly in deoxygenated solutions, whereas in oxygenated solution a steady state was reached once approximately 70% of the iron(III) was reduced.[25]

Chamber Experiments. Figure 4 summarizes the evolution of organic aerosol and gas-phase glycolaldehyde concentrations during chamber photooxidation experiments. Organic mass is presented as the ratio of Org/SO_4 to minimize uncertainties in particle wall loss, HR-AMS collection efficiencies, and line losses. Across all experiments, the glycolaldehyde signal decays after the initiation of photochemistry. The glycolaldehyde decay rate is comparable among all experiments. Glycolaldehyde will photolyze in the Caltech chamber with a photolysis rate constant of $j_{Gly} = 2.1 \times 10^{-6}$ s^{-1}. Furthermore, glycolaldehyde photolysis leads to reactive products, such as formaldehyde, that promote OH formation and enhance glycolaldehyde decay.[70] In experiments absent of seed, glycolaldehyde decay is well-represented by a simple photochemical model (see Supporting Information); thus, the bulk of glycolaldehyde decay is attributable to nonheterogeneous processes.

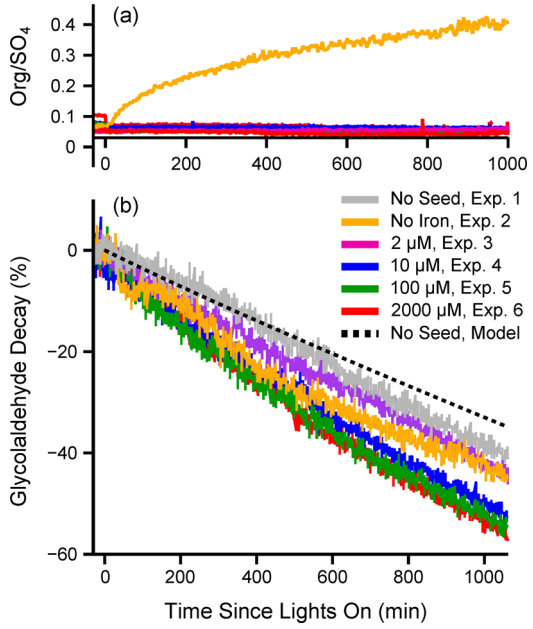

Figure 4. Measurements of (a) aerosol Org/SO_4 ratios and (b) gas-phase glycolaldehyde during chamber experiments. Organic aerosol formation is suppressed when iron is present in the seed aerosol (a). Enhanced particle-phase iron concentrations lead to greater glycolaldehyde decay (b); however, most of the glycolaldehyde decay is determined by gas-phase photochemical processes (no seed, model).

For seeded experiments doped with low concentrations of iron (exp. 2 and 3), the loss of glycolaldehyde after 1000 min is comparable to that of exp. 1. In contrast, seeded experiments doped with high concentrations of iron (exp. 4−6) exhibit an additional ∼10% decrease in glycolaldehyde. These modest increases in glycolaldehyde decay may reflect enhanced losses due to particle-phase oxidation in the presence of iron. Gas-particle partitioning in systems such as glycolaldehyde and glyoxal, which participate in dark particle-phase reactions to form diols, hemiacetals, and amines/imines,[26,71] is kinetically limited.[1,26,72,73] Enhanced heterogeneous reactions would increase the rate of VOC partitioning and consequently deplete gas-phase concentrations. We note, however, that these processes likely play a small role in comparison to glycolaldehyde photolysis.

The impact of ferrioxalate photochemistry is most pronounced on organic aerosol concentrations. Figure 4a illustrates organic aerosol growth for systems doped with various concentrations of iron. In experiments absent of iron, organic aerosol is observed to increase upon the initiation of photochemistry. As demonstrated in Figure S2, this growth (and simultaneous gas-phase glycolaldehyde decay) stops when lights are turned off. In the Supporting Information, we demonstrate that ∼50% of the decay in gas-phase glycolaldehyde is likely attributable to the reaction with OH. Glycolaldehyde reacts with OH in the gas phase to form glyoxal at high yields (∼22%).[70] Using the photochemical box model, we estimate that 3.5 ppb of glyoxal could have formed as a result of glycolaldehyde photochemistry. Previous studies have shown that glyoxal efficiently forms SOA on ammonium sulfate seed under dark and irradiated conditions.[73−75] Kampf et al. observed 0.75 $\mu g\ m^{-3}$ of SOA formation in the presence of low glycolaldehyde concentrations (∼10 ppb).[76] The authors performed these experiments under conditions similar to those described here. We hypothesize that a significant fraction of SOA formed during iron-free experiments could have resulted from glyoxal partitioning; however, quantification of glyoxal SOA is beyond the scope of this study.

In systems doped with iron, organic aerosol growth is inhibited. Even for the lowest concentrations of iron, we observe no noticeable increase in organic aerosol concentrations. This growth inhibition may result from a number of processes. First, glycolaldehyde was likely oxidized in the particle according to the reactions outlined by Scheme 1 to form CO_2 and other volatile species. This pathway is supported by FIDI-MS experiments in which glyoxal, glycolic acid, and glyoxylic acid form shortly after irradiation. Second, it is possible that oligomerization processes were interrupted because of the oxidation of hydrated glyoxal monomers or glycolaldehyde monomers. As discussed for FIDI-MS experiments, glyoxal diols can be oxidized by OH to form oxalic acid via the glyoxylic acid pathway.[4] This oxidation could shift oligomer equilibrium and consequently lead to a loss of SOA.

The proposed chamber mechanism is consistent with known heterogeneous reactions for glyoxal and glycolaldehyde.[3,4,13,14] It is notable that several oxidation pathways can lead to the formation of oxalic acid. With additional oxalic acid, ferrioxalate complexes would likely reform and subsequently lead to the recycling of hydroxyl radicals. We hypothesize that this process could set up a catalytic cycle that would ultimately lead to the destruction of SOA precursors (such as glyoxal diols). This inhibition mechanism is consistent with the lack of SOA formed in any experiment performed with iron-containing aerosols.

Previous studies have demonstrated that iron chemistry has notable impacts on organic aerosol consumption and/or inhibition. Using dark Fenton chemistry as a source of OH, Daumit et al. oxidized suspended particles of polyols and observed substantial loss of carbon to the gas phase.[75] The

DOI: 10.1021/acs.est.6b03588
Environ. Sci. Technol. 2016, 50, 12241−12249

authors demonstrated that the product distributions in suspended particles were substantially different than those observed in bulk solutions due to the differences in liquid water content. Chu et al. conducted conventional SOA yield experiments in the presence of inorganic seed and found substantial reduction in SOA formation in systems containing $FeSO_4$.[27] The authors attribute these observations to iron reduction reactions and interruption of dark accretion reactions; however, losses are also likely to occur as a result of photooxidation of iron-organic complexes.

The studies described above were conducted using seed composed of pure $FeSO_4$. The results presented here indicate that even a trace amount of iron (0.005 wt %) has the potential to strongly impact aerosol composition. Ferrioxalate chemistry is likely to apply to other aqueous systems where oxalic acid is produced in large abundance. In addition, these results demonstrate that oxidation products in aqueous organic systems, such as oxalate formed by the OH + glycolaldehyde mechanism, may participate in the recycling of oxidizing species and subsequent oxidation of dissolved organic material. Further laboratory investigations into the role of iron(III) oxalate photochemistry in reactive uptake, along with additional field measurements, are necessary to better constrain the role of such complexes in aqueous tropospheric photochemistry.

■ ASSOCIATED CONTENT

Supporting Information

The Supporting Information is available free of charge on the ACS Publications website at DOI: 10.1021/acs.est.6b03588.

Materials used in experiments, design of FIDI-MS apparatus, environmental chamber protocol, predicted equilibrium complexes of iron, FIDI-MS control experiments, and details of the photochemical box model (PDF)

■ AUTHOR INFORMATION

Corresponding Author

*Phone: 626-395-6525. Fax: 626-395-4912. E-mail: jlbchamp@caltech.edu.

Present Addresses

[¶]M.M.C.: Cooperative Institute for Research in Environmental Sciences, Boulder, CO, 80309, USA.

[‖]K.A.S.: U.S. Army Criminal Investigation Laboratory, Fort Gillem, GA, 30297, USA.

Author Contributions

D.AT. and M.M.C. contributed equally to this work. The manuscript was written through contributions of all authors. All authors have given approval to the final version of the manuscript.

Notes

The authors declare no competing financial interest.

■ ACKNOWLEDGMENTS

This work was supported by the Beckman Institute at Caltech and by the NSF grants CHE-1508825 and AGS-1523500. K.A.S. acknowledges support from the Department of Defense SMART program. The authors thank Kevin M. Barraza, Xinxing Zhang, and Prof. Mitchio Okumura for assistance with radiant flux measurements.

■ REFERENCES

(1) Herrmann, H.; Schaefer, T.; Tilgner, A.; Styler, S. A.; Weller, C.; Teich, M.; Otto, T. Tropospheric Aqueous-Phase Chemistry: Kinetics, Mechanisms, and Its Coupling to a Changing Gas Phase. *Chem. Rev.* **2015**, *115* (10), 4259−4334.

(2) Blando, J. D.; Turpin, B. J. Secondary organic aerosol formation in cloud and fog droplets: a literature evaluation of plausibility. *Atmos. Environ.* **2000**, *34* (10), 1623−1632.

(3) Ervens, B.; Turpin, B. J.; Weber, R. J. Secondary organic aerosol formation in cloud droplets and aqueous particles (aqSOA): a review of laboratory, field and model studies. *Atmos. Chem. Phys.* **2011**, *11* (21), 11069−11102.

(4) Lim, Y. B.; Tan, Y.; Perri, M. J.; Seitzinger, S. P.; Turpin, B. J. Aqueous chemistry and its role in secondary organic aerosol (SOA) formation. *Atmos. Chem. Phys.* **2010**, *10* (21), 10521−10539.

(5) McNeill, V. F. Aqueous Organic Chemistry in the Atmosphere: Sources and Chemical Processing of Organic Aerosols. *Environ. Sci. Technol.* **2015**, *49* (3), 1237−1244.

(6) Ervens, B.; Volkamer, R. Glyoxal processing by aerosol multiphase chemistry: towards a kinetic modeling framework of secondary organic aerosol formation in aqueous particles. *Atmos. Chem. Phys.* **2010**, *10* (17), 8219−8244.

(7) Jang, M.; Czoschke, N. M.; Lee, S.; Kamens, R. M. Heterogeneous Atmospheric Aerosol Production by Acid-Catalyzed Particle-Phase Reactions. *Science* **2002**, *298* (5594), 814−817.

(8) Vione, D.; Maurino, V.; Minero, C.; Pelizzetti, E.; Harrison, M. A. J.; Olariu, R.-I.; Arsene, C. Photochemical reactions in the tropospheric aqueous phase and on particulate matter. *Chem. Soc. Rev.* **2006**, *35* (5), 441−453.

(9) George, C.; Ammann, M.; D'Anna, B.; Donaldson, D. J.; Nizkorodov, S. A. Heterogeneous Photochemistry in the Atmosphere. *Chem. Rev.* **2015**, *115* (10), 4218−4258.

(10) George, C.; D'Anna, B.; Herrmann, H.; Weller, C.; Vaida, V.; Donaldson, D. J.; Bartels-Rausch, T.; Ammann, M. Emerging Areas in Atmospheric Photochemistry. In *Atmospheric and Aerosol Chemistry*; McNeill, F. V., Ariya, A. P., Eds.; Springer: Berlin, 2014; pp 1−53.

(11) Ervens, B.; Sorooshian, A.; Lim, Y. B.; Turpin, B. J. Key parameters controlling OH-initiated formation of secondary organic aerosol in the aqueous phase (aqSOA). *J. Geophys. Res.: Atmos.* **2014**, *119* (7), 3997−4016.

(12) Carlton, A. G.; Turpin, B. J.; Altieri, K. E.; Seitzinger, S.; Reff, A.; Lim, H.-J.; Ervens, B. Atmospheric oxalic acid and SOA production from glyoxal: Results of aqueous photooxidation experiments. *Atmos. Environ.* **2007**, *41* (35), 7588−7602.

(13) Perri, M. J.; Seitzinger, S.; Turpin, B. J. Secondary organic aerosol production from aqueous photooxidation of glycolaldehyde: Laboratory experiments. *Atmos. Environ.* **2009**, *43* (8), 1487−1497.

(14) Perri, M. J.; Lim, Y. B.; Seitzinger, S. P.; Turpin, B. J. Organosulfates from glycolaldehyde in aqueous aerosols and clouds: Laboratory studies. *Atmos. Environ.* **2010**, *44* (21−22), 2658−2664.

(15) Zhang, X.; Chen, Z. M.; Zhao, Y. Laboratory simulation for the aqueous OH-oxidation of methyl vinyl ketone and methacrolein: significance to the in-cloud SOA production. *Atmos. Chem. Phys.* **2010**, *10* (19), 9551−9561.

(16) Aregahegn, K. Z.; Noziere, B.; George, C. Organic aerosol formation photo-enhanced by the formation of secondary photosensitizers in aerosols. *Faraday Discuss.* **2013**, *165* (0), 123−134.

(17) Griffith, E. C.; Carpenter, B. K.; Shoemaker, R. K.; Vaida, V. Photochemistry of aqueous pyruvic acid. *Proc. Natl. Acad. Sci. U. S. A.* **2013**, *110* (29), 11714−11719.

(18) Fu, H.; Ciuraru, R.; Dupart, Y.; Passananti, M.; Tinel, L.; Rossignol, S.; Perrier, S.; Donaldson, D. J.; Chen, J.; George, C. Photosensitized Production of Atmospherically Reactive Organic Compounds at the Air/Aqueous Interface. *J. Am. Chem. Soc.* **2015**, *137* (26), 8348−8351.

(19) Wang, Z.; Chen, C.; Ma, W.; Zhao, J. Photochemical Coupling of Iron Redox Reactions and Transformation of Low-Molecular-Weight Organic Matter. *J. Phys. Chem. Lett.* **2012**, *3* (15), 2044−2051.

DOI: 10.1021/acs.est.6b03588
Environ. Sci. Technol. 2016, 50, 12241−12249

(20) Harris, E.; Sinha, B.; van Pinxteren, D.; Tilgner, A.; Fomba, K. W.; Schneider, J.; Roth, A.; Gnauk, T.; Fahlbusch, B.; Mertes, S.; Lee, T.; Collett, J.; Foley, S.; Borrmann, S.; Hoppe, P.; Herrmann, H. Enhanced Role of Transition Metal Ion Catalysis During In-Cloud Oxidation of SO2. *Science* **2013**, *340* (6133), 727−730.
(21) Guasco, T. L.; Cuadra-Rodriguez, L. A.; Pedler, B. E.; Ault, A. P.; Collins, D. B.; Zhao, D.; Kim, M. J.; Ruppel, M. J.; Wilson, S. C.; Pomeroy, R. S.; Grassian, V. H.; Azam, F.; Bertram, T. H.; Prather, K. A. Transition Metal Associations with Primary Biological Particles in Sea Spray Aerosol Generated in a Wave Channel. *Environ. Sci. Technol.* **2014**, *48* (2), 1324−1333.
(22) Sorooshian, A.; Wang, Z.; Coggon, M. M.; Jonsson, H. H.; Ervens, B. Observations of Sharp Oxalate Reductions in Stratocumulus Clouds at Variable Altitudes: Organic Acid and Metal Measurements During the 2011 E-PEACE Campaign. *Environ. Sci. Technol.* **2013**, *47* (14), 7747−7756.
(23) Deguillaume, L.; Leriche, M.; Desboeufs, K.; Mailhot, G.; George, C.; Chaumerliac, N. Transition Metals in Atmospheric Liquid Phases: Sources, Reactivity, and Sensitive Parameters. *Chem. Rev.* **2005**, *105* (9), 3388−3431.
(24) Faust, B. C.; Hoigné, J. Photolysis of Fe (III)-hydroxy complexes as sources of OH radicals in clouds, fog and rain. *Atmos. Environ., Part A* **1990**, *24* (1), 79−89.
(25) Zuo, Y.; Hoigne, J. Formation of hydrogen peroxide and depletion of oxalic acid in atmospheric water by photolysis of iron(III)-oxalato complexes. *Environ. Sci. Technol.* **1992**, *26* (5), 1014−1022.
(26) Nguyen, T. B.; Coggon, M. M.; Flagan, R. C.; Seinfeld, J. H. Reactive Uptake and Photo-Fenton Oxidation of Glycolaldehyde in Aerosol Liquid Water. *Environ. Sci. Technol.* **2013**, *47* (9), 4307−4316.
(27) Chu, B.; Hao, J.; Takekawa, H.; Li, J.; Wang, K.; Jiang, J. The remarkable effect of $FeSO_4$ seed aerosols on secondary organic aerosol formation from photooxidation of α-pinene/NO_x and toluene/NO_x. *Atmos. Environ.* **2012**, *55*, 26−34.
(28) Xiao, D.; Guo, Y.; Lou, X.; Fang, C.; Wang, Z.; Liu, J. Distinct effects of oxalate versus malonate on the iron redox chemistry: Implications for the photo-Fenton reaction. *Chemosphere* **2014**, *103* (0), 354−358.
(29) Wang, Z.; Xiao, D.; Liu, J. Diverse redox chemistry of photo/ferrioxalate system. *RSC Adv.* **2014**, *4* (84), 44654−44658.
(30) Balmer, M. E.; Sulzberger, B. Atrazine Degradation in Irradiated Iron/Oxalate Systems: Effects of pH and Oxalate. *Environ. Sci. Technol.* **1999**, *33* (14), 2418−2424.
(31) Weller, C.; Horn, S.; Herrmann, H. Effects of Fe(III)-concentration, speciation, excitation-wavelength and light intensity on the quantum yield of iron(III)-oxalato complex photolysis. *J. Photochem. Photobiol., A* **2013**, *255*, 41−49.
(32) Weller, C.; Horn, S.; Herrmann, H. Photolysis of Fe(III) carboxylato complexes: Fe(II) quantum yields and reaction mechanisms. *J. Photochem. Photobiol., A* **2013**, *268*, 24−36.
(33) Sorooshian, A.; Ng, N. L.; Chan, A. W. H.; Feingold, G.; Flagan, R. C.; Seinfeld, J. H. Particulate organic acids and overall water-soluble aerosol composition measurements from the 2006 Gulf of Mexico Atmospheric Composition and Climate Study (GoMACCS). *J. Geophys. Res.: Atmos.* **2007**, *112* (D13), D13201.
(34) Benedict, K. B.; Lee, T.; Collett, J. L., Jr Cloud water composition over the southeastern Pacific Ocean during the VOCALS regional experiment. *Atmos. Environ.* **2012**, *46*, 104−114.
(35) Sorooshian, A.; Lu, M.-L.; Brechtel, F. J.; Jonsson, H.; Feingold, G.; Flagan, R. C.; Seinfeld, J. H. On the Source of Organic Acid Aerosol Layers above Clouds. *Environ. Sci. Technol.* **2007**, *41* (13), 4647−4654.
(36) Parker, C. A. A New Sensitive Chemical Actinometer. I. Some Trials with Potassium Ferrioxalate. *Proc. R. Soc. London, Ser. A* **1953**, *220* (1140), 104−116.
(37) Hatchard, C. G.; Parker, C. A. A New Sensitive Chemical Actinometer. II. Potassium Ferrioxalate as a Standard Chemical Actinometer. *Proc. R. Soc. London, Ser. A* **1956**, *235* (1203), 518−536.
(38) Long, Y.; Charbouillot, T.; Brigante, M.; Mailhot, G.; Delort, A.-M.; Chaumerliac, N.; Deguillaume, L. Evaluation of modeled cloud chemistry mechanism against laboratory irradiation experiments: The HxOy/iron/carboxylic acid chemical system. *Atmos. Environ.* **2013**, *77*, 686−695.
(39) Vincze, L.; Papp, S. Individual quantum yields of Fe3+OXn2−Hm+ complexes in aqueous acidic solutions ($OX^{2-} \equiv C_2O_4^{2-}$, n = 1 − 3, m = 0,1). *J. Photochem.* **1987**, *36* (3), 289−296.
(40) Chen, J.; Zhang, H.; Tomov, I. V.; Rentzepis, P. M. Electron Transfer Mechanism and Photochemistry of Ferrioxalate Induced by Excitation in the Charge Transfer Band. *Inorg. Chem.* **2008**, *47* (6), 2024−2032.
(41) Pozdnyakov, I. P.; Kel, O. V.; Plyusnin, V. F.; Grivin, V. P.; Bazhin, N. M. New Insight into Photochemistry of Ferrioxalate. *J. Phys. Chem. A* **2008**, *112* (36), 8316−8322.
(42) Chen, J.; Dvornikov, A. S.; Rentzepis, P. M. Comment on "New Insight into Photochemistry of Ferrioxalate". *J. Phys. Chem. A* **2009**, *113* (30), 8818−8819.
(43) Pozdnyakov, I. P.; Kel, O. V.; Plyusnin, V. F.; Grivin, V. P.; Bazhin, N. M. Reply to "Comment on 'New insight into Photochemistry of Ferrioxalate'". *J. Phys. Chem. A* **2009**, *113* (30), 8820−8822.
(44) Sedlak, D. L.; Hoigné, J. The role of copper and oxalate in the redox cycling of iron in atmospheric waters. *Atmos. Environ., Part A* **1993**, *27* (14), 2173−2185.
(45) Zuo, Y.; Zhan, J. Effects of oxalate on Fe-catalyzed photooxidation of dissolved sulfur dioxide in atmospheric water. *Atmos. Environ.* **2005**, *39* (1), 27−37.
(46) Spaulding, R. S.; Schade, G. W.; Goldstein, A. H.; Charles, M. J. Characterization of secondary atmospheric photooxidation products: Evidence for biogenic and anthropogenic sources. *J. Geophys. Res.* **2003**, *108* (D8), 4247.
(47) Atkinson, R.; Arey, J. Atmospheric Chemistry of Biogenic Organic Compounds. *Acc. Chem. Res.* **1998**, *31* (9), 574−583.
(48) Betterton, E. A.; Hoffmann, M. R. Henry's law constants of some environmentally important aldehydes. *Environ. Sci. Technol.* **1988**, *22* (12), 1415−1418.
(49) Grimm, R. L.; Beauchamp, J. L. Field-Induced Droplet Ionization Mass Spectrometry. *J. Phys. Chem. B* **2003**, *107* (51), 14161−14163.
(50) Grimm, R. L.; Hodyss, R.; Beauchamp, J. L. Probing Interfacial Chemistry of Single Droplets with Field-Induced Droplet Ionization Mass Spectrometry: Physical Adsorption of Polycyclic Aromatic Hydrocarbons and Ozonolysis of Oleic Acid and Related Compounds. *Anal. Chem.* **2006**, *78* (11), 3800−3806.
(51) Loza, C. L.; Craven, J. S.; Yee, L. D.; Coggon, M. M.; Schwantes, R. H.; Shiraiwa, M.; Zhang, X.; Schilling, K. A.; Ng, N. L.; Canagaratna, M. R.; Ziemann, P. J.; Flagan, R. C.; Seinfeld, J. H. Secondary organic aerosol yields of 12-carbon alkanes. *Atmos. Chem. Phys.* **2014**, *14* (3), 1423−1439.
(52) Zhang, X.; Schwantes, R. H.; Coggon, M. M.; Loza, C. L.; Schilling, K. A.; Flagan, R. C.; Seinfeld, J. H. Role of ozone in SOA formation from alkane photooxidation. *Atmos. Chem. Phys.* **2014**, *14* (3), 1733−1753.
(53) Grimm, R. L.; Beauchamp, J. L. Dynamics of Field-Induced Droplet Ionization: Time-Resolved Studies of Distortion, Jetting, and Progeny Formation from Charged and Neutral Methanol Droplets Exposed to Strong Electric Fields. *J. Phys. Chem. B* **2005**, *109* (16), 8244−8250.
(54) Kebarle, P.; Verkerk, U. H. Electrospray: From ions in solution to ions in the gas phase, what we know now. *Mass Spectrom. Rev.* **2009**, *28* (6), 898−917.
(55) Smith, J. N.; Flagan, R. C.; Beauchamp, J. L. Droplet Evaporation and Discharge Dynamics in Electrospray Ionization. *J. Phys. Chem. A* **2002**, *106* (42), 9957−9967.
(56) Neidholdt, E. L. Novel pyroelectric and switched ferroelectric ion sources in mass spectrometry: implementation and applications. Ph.D. Dissertation California Institute of Technology, Pasadena, CA, 2010.

DOI: 10.1021/acs.est.6b03588
Environ. Sci. Technol. 2016, 50, 12241−12249

(57) DeMore, W. B.; Sander, S. P.; Golden, D. B.; Hampson, R. F.; Kurylo, M. J.; Howard, C. J.; Ravishankara, A. R.; Kolb, C. E.; Molina, M. J. *Chemical Kinetics and Photochemical Data for Use in Stratospheric Modeling*, Evaluation Number 12, JPL Pub. 97-4; NASA Jet Propulsion Laboratory: Pasadena, CA, 1997.
(58) Drewnick, F.; Hings, S. S.; DeCarlo, P.; Jayne, J. T.; Gonin, M.; Fuhrer, K.; Weimer, S.; Jimenez, J. L.; Demerjian, K. L.; Borrmann, S.; Worsnop, D. R. A New Time-of-Flight Aerosol Mass Spectrometer (TOF-AMS)—Instrument Description and First Field Deployment. *Aerosol Sci. Technol.* **2005**, *39* (7), 637−658.
(59) DeCarlo, P. F.; Kimmel, J. R.; Trimborn, A.; Northway, M. J.; Jayne, J. T.; Aiken, A. C.; Gonin, M.; Fuhrer, K.; Horvath, T.; Docherty, K. S.; Worsnop, D. R.; Jimenez, J. L. Field-Deployable, High-Resolution, Time-of-Flight Aerosol Mass Spectrometer. *Anal. Chem.* **2006**, *78* (24), 8281−8289.
(60) Aiken, A. C.; DeCarlo, P. F.; Kroll, J. H.; Worsnop, D. R.; Huffman, J. A.; Docherty, K. S.; Ulbrich, I. M.; Mohr, C.; Kimmel, J. R.; Sueper, D.; Sun, Y.; Zhang, Q.; Trimborn, A.; Northway, M.; Ziemann, P. J.; Canagaratna, M. R.; Onasch, T. B.; Alfarra, M. R.; Prevot, A. S. H.; Dommen, J.; Duplissy, J.; Metzger, A.; Baltensperger, U.; Jimenez, J. L. O/C and OM/OC Ratios of Primary, Secondary, and Ambient Organic Aerosols with High-Resolution Time-of-Flight Aerosol Mass Spectrometry. *Environ. Sci. Technol.* **2008**, *42* (12), 4478−4485.
(61) Canagaratna, M. R.; Jimenez, J. L.; Kroll, J. H.; Chen, Q.; Kessler, S. H.; Massoli, P.; Hildebrandt Ruiz, L.; Fortner, E.; Williams, L. R.; Wilson, K. R.; Surratt, J. D.; Donahue, N. M.; Jayne, J. T.; Worsnop, D. R. Elemental ratio measurements of organic compounds using aerosol mass spectrometry: characterization, improved calibration, and implications. *Atmos. Chem. Phys.* **2015**, *15* (1), 253−272.
(62) Crounse, J. D.; McKinney, K. A.; Kwan, A. J.; Wennberg, P. O. Measurement of Gas-Phase Hydroperoxides by Chemical Ionization Mass Spectrometry. *Anal. Chem.* **2006**, *78* (19), 6726−6732.
(63) St. Clair, J. M.; McCabe, D. C.; Crounse, J. D.; Steiner, U.; Wennberg, P. O. Chemical ionization tandem mass spectrometer for the in situ measurement of methyl hydrogen peroxide. *Rev. Sci. Instrum.* **2010**, *81* (9), 094102.
(64) Bianco, A.; Passananti, M.; Perroux, H.; Voyard, G.; Mouchel-Vallon, C.; Chaumerliac, N.; Mailhot, G.; Deguillaume, L.; Brigante, M. A better understanding of hydroxyl radical photochemical sources in cloud waters collected at the puy de Dôme station − experimental versus modelled formation rates. *Atmos. Chem. Phys.* **2015**, *15* (16), 9191−9202.
(65) Hämeri, K.; Väkevä, M.; Hansson, H.-C.; Laaksonen, A. Hygroscopic growth of ultrafine ammonium sulphate aerosol measured using an ultrafine tandem differential mobility analyzer. *J. Geophys. Res.: Atmos.* **2000**, *105* (D17), 22231−22242.
(66) Schweitzer, F.; Magi, L.; Mirabel, P.; George, C. Uptake Rate Measurements of Methanesulfonic Acid and Glyoxal by Aqueous Droplets. *J. Phys. Chem. A* **1998**, *102* (3), 593−600.
(67) Hastings, W. P.; Koehler, C. A.; Bailey, E. L.; De Haan, D. O. Secondary Organic Aerosol Formation by Glyoxal Hydration and Oligomer Formation: Humidity Effects and Equilibrium Shifts during Analysis. *Environ. Sci. Technol.* **2005**, *39* (22), 8728−8735.
(68) Yu, G.; Bayer, A. R.; Galloway, M. M.; Korshavn, K. J.; Fry, C. G.; Keutsch, F. N. Glyoxal in Aqueous Ammonium Sulfate Solutions: Products, Kinetics and Hydration Effects. *Environ. Sci. Technol.* **2011**, *45* (15), 6336−6342.
(69) Ortiz-Montalvo, D. L.; Lim, Y. B.; Perri, M. J.; Seitzinger, S. P.; Turpin, B. J. Volatility and Yield of Glycolaldehyde SOA Formed through Aqueous Photochemistry and Droplet Evaporation. *Aerosol Sci. Technol.* **2012**, *46* (9), 1002−1014.
(70) Magneron, I.; Mellouki, A.; Le Bras, G.; Moortgat, G. K.; Horowitz, A.; Wirtz, K. Photolysis and OH-Initiated Oxidation of Glycolaldehyde under Atmospheric Conditions. *J. Phys. Chem. A* **2005**, *109* (20), 4552−4561.
(71) Barsanti, K. C.; Pankow, J. F. Thermodynamics of the formation of atmospheric organic particulate matter by accretion reactions—Part 1: aldehydes and ketones. *Atmos. Environ.* **2004**, *38* (26), 4371−4382.
(72) Liu, Y.; Liggio, J.; Staebler, R.; Li, S. M. Reactive uptake of ammonia to secondary organic aerosols: kinetics of organonitrogen formation. *Atmos. Chem. Phys.* **2015**, *15* (23), 13569−13584.
(73) Galloway, M. M.; Chhabra, P. S.; Chan, A. W. H.; Surratt, J. D.; Flagan, R. C.; Seinfeld, J. H.; Keutsch, F. N. Glyoxal uptake on ammonium sulphate seed aerosol: reaction products and reversibility of uptake under dark and irradiated conditions. *Atmos. Chem. Phys.* **2009**, *9* (10), 3331−3345.
(74) Kroll, J. H.; Ng, N. L.; Murphy, S. M.; Varutbangkul, V.; Flagan, R. C.; Seinfeld, J. H. Chamber studies of secondary organic aerosol growth by reactive uptake of simple carbonyl compounds. *J. Geophys. Res.* **2005**, *110* (D23), D23207.
(75) Daumit, K. E.; Carrasquillo, A. J.; Hunter, J. F.; Kroll, J. H. Laboratory studies of the aqueous-phase oxidation of polyols: submicron particles vs. bulk aqueous solution. *Atmos. Chem. Phys.* **2014**, *14* (19), 10773−10784.
(76) Kampf, C. J.; Waxman, E. M.; Slowik, J. G.; Dommen, J.; Pfaffenberger, L.; Praplan, A. P.; Prévôt, A. S. H.; Baltensperger, U.; Hoffmann, T.; Volkamer, R. Effective Henry's Law Partitioning and the Salting Constant of Glyoxal in Aerosols Containing Sulfate. *Environ. Sci. Technol.* **2013**, *47* (9), 4236−4244.

DOI: 10.1021/acs.est.6b03588
Environ. Sci. Technol. 2016, 50, 12241−12249